Chapter 10

Spin-Orbit Coupling at Magnetic Metal Surfaces

In this chapter we present experimental data of surface states on magnetic rare-earth metals, including their analysis and discussion, with special emphasis on spin-orbit interaction.

One motivation for this work has been the fast growing field of semiconductor spintronics, where the manipulation of electron spins is one of the central topics [89]. Most of the schemes proposed for computing with electron spins, e.g. using quantum dots (QDs), are based on time-dependent magnetic fields. However, it would be highly preferable for applications to use time-dependent electric fields instead of magnetic ones, and various mechanisms of spin-orbit interaction have been proposed [17], which open attractive possibilities for electric spin control. Recently, Kato et al. [90] demonstrated manipulation of electron spins in a 2D system with Gigahertz electric fields. This experimental success raises questions about the dominant physical mechanisms controlling the coupling of spins to the electric field, and about the key properties of the medium that are required for an effective spin-orbit coupling (SOC).

All necessary conditions for SOC are fulfilled at the crystal surface. There is a structural asymmetry as well as a potential gradient created by the charge distribution at the metal/vacuum interface. Many surfaces exhibit electronic states that are localized in the near-surface region, and are therefore natural choices for an investigation of Rashba spin-orbit interaction. Localized near the surface, they represent a nice example of a quasi two-dimensional electron system, which is in many aspects similar to the free-electron gas confined in a 2D quantum well; it can be considered as a prototype system for investigating the physical mechanism of spin coupling to the electric field.

In this work, we have investigated the Rashba spin-orbit coupling at the surface of gadolinium and terbium metal as well as their surface oxides. These systems exhibit a substantial Rashba effect, extending the class of surfaces that exhibit Rashba splitting. Our findings lead to the conclusion that the Rashba effect is a rather general surface and interface phenomenon, playing an important role at metal surfaces that contain atoms of high Z (atomic number).

For the discussion of the Rashba effect at magnetic metal surfaces it is im-

portant to keep in mind that magnetism split the electron energy levels by means of exchange interaction, which also defines the spin polarization of the states. This leads to two important consequences for the appearance of the Rashba effect: first, the electrons spins are ordered along a common quantization axis defined by the magnetization orientation; second, the spin degeneracy is removed by exchange. Therefore the Rashba interaction cannot lead to a further splitting of the state as in the case of nonmagnetic surfaces, but to the modification of the energy dispersion curves. The experimental geometry chosen for our experiments (see Fig. 3.8) provides the orthogonal orientations of the electric field vector, the spin and the wave vectors of the electrons. Therefore a magnetization reversal will result in the two opposite limiting cases for the Rashba spin-orbit interaction. Being superimposed corresponding dispersion curves present the Rashba splitting, similar to nonmagnetic case.

10.1 The Gd(0001) surface

Experiment

Gadolinium is one of the four ferromagnetic elementary metals (Fe, Co, Ni, and Gd). They have been studied extensively. There is also a long history of experimental and theoretical studies devoted to the magnetic properties of their surfaces, of which the Gd surface has received particular attention over the past decade [54–59].

Our photoemission studies of the spin-polarized surface state at the Gd(0001) surface presented below reveal that its energy dispersion depends on the orientation of the spin-quantization axis of the electron relative to its propagation direction in the electric field provided by the surface potential: this gives rise to a sizeable Rashba effect.

Photoemission data of the Gd valence band with high angular and energy resolution are presented in Fig. 10.1. The set of experimental spectra (energy distribution curves, EDC) display the energy dispersion of the valence bands near the $\overline{\Gamma}$ point of the Brillouin zone, in the $\overline{\Gamma} - \overline{M}$ azimuth, covering the investigated region with constant angular steps. The inset shows the fit of the spectrum corresponding to the $\overline{\Gamma}$ point. The most intense peak close to the Fermi level represents the majority part of d_{z^2} surface state of gadolinium, that is exchange split in the ferromagnetic state below T_c =293 K [63, 68]. The minority part is located above the Fermi level and is not accessible to photoemission. The two features at binding energies of 1.2 eV and 2.2 eV represent the exchange-split Σ_2 bulk band. As shown in Fig. 10.1, the surface state disperses downwards, away from the Fermi level, and is rather flat near $\overline{\Gamma}$. By contrast, the Σ_2 band shows an upward dispersion towards the Fermi level.

The effect of a magnetization reversal on the surface-state binding energy is illustrated in Fig. 10.2. For the off-normal emission we observe a clear shift of the peak position maxima upon magnetization change, while in normal emission the peak position is the same for both magnetization directions. The spectral positions of the peak maxima, and hence the angle-resoved binding energy of the states can be obtained very accurately, from the spectra in Fig. 10.1 allowing

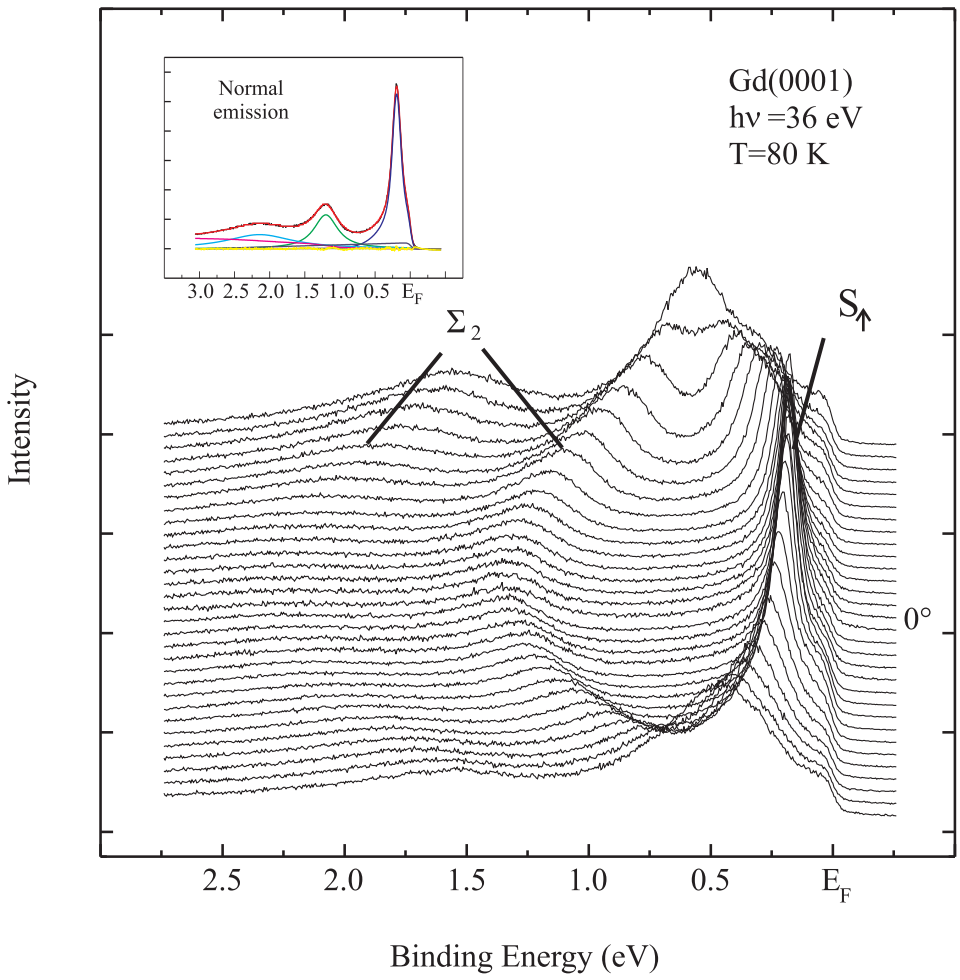

Figure 10.1: (a) Energy-distribution curves of the valence-band region of Gd(0001) near the $\overline{\Gamma}$ point along $\overline{\Gamma} - \overline{M}$, plotted for angular steps of 0.55°; the spectra were measured with 36-eV photons. Characteristic features of the valence band are the majority-spin surface state ($S_\uparrow$) and the exchange-split Σ_2 band. The inset displays the normal-emission spectrum with the results of a fit analysis.

us to map the energy dispersions $E(k)$ of the surface state.

The dispersion of the Gd(0001) surface states near the center of the surface Brillouin zone in $\overline{\Gamma} \rightarrow \overline{M}$ direction, derived from the spectra in Fig.10.1 and a similar data set with reversed magnetisation, is shown in Fig. 10.3. Solid and hollow circles represent the surface-state dispersion for the two opposite magnetization directions, which were chosen to be orthogonal to the electron momentum $k_{||}$ in order to maximize the Rashba interaction, cf. Eq. 9.2. Two distinctly different dispersions are observed for the oppositely magnetized surface. In the narrow region around $\overline{\Gamma}$, the dispersion is nearly parabolic, although it is known

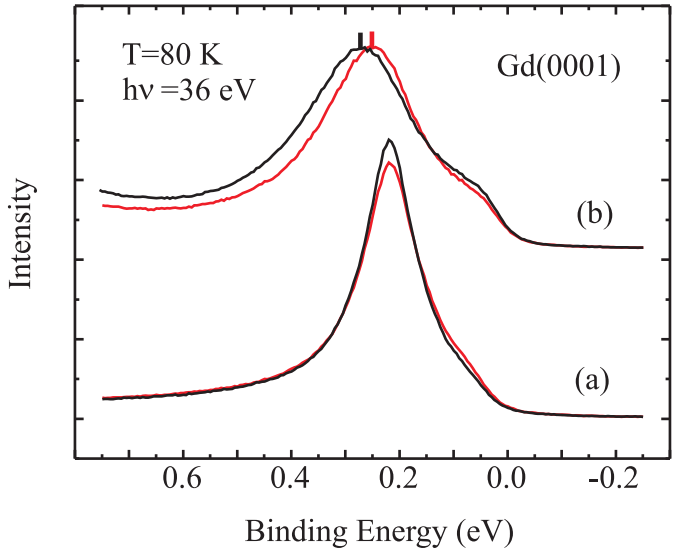

Figure 10.2: Effects of magnetization reversal (red and black curves) on the peak position of the Gd(0001) surface state in the (a) normal-emission ($\alpha = 0°$) and (b) off-normal-emission ($\alpha = 6°$) photoemission spectrum.

that (in contrast to sp-like surface states) the dispersion of this state is rather flat in the center of the Brillouin zone (BZ). Both data sets were simultaneously fitted with quadratic functions, with the results presented by solid lines. The $k_{\|}$ – difference of electrons with equal energies is found to be 0.029 ± 0.002 Å^{-1}, which represents a symmetric shift of $\left|\Delta k_{\|}\right| = 0.015 \pm 0.002$ Å^{-1} of each band with respect to the zone center. The energy difference $\Delta\epsilon$ between surface state peaks with equal $k_{\|}$ are displayed in Fig.10.3(b). From it's zero crossing at $\overline{\Gamma}$, the magnitude of the surface-state splitting increases with $k_{\|}$ in $\overline{\Gamma} \rightarrow \overline{M}$ direction. Such a behavior agrees very well with expectations on the basis of the Rashba Hamiltonian: we therefore explain the appearance of two different dispersions as a consequence of the Rashba effect [91].

For a correct interpretation and in order to unravel the main contributions to this sizeable effect, it is worthwhile to compare the experimental data with band-structure calculations performed by G. Bihlmayer, Forschungszentrum Jülich.

Ab-initio calculations: Gd

From a theoretical point of view, gadolinium metal is a model system for testing new relativistic theoretical methods, mainly due to the combination of ferromagnetism and the relevance of relativistic effects. Even today, the description of Gd is a challenge for first-principles theory [92], mainly due to the localized nature of the 4f electrons that lie in the same energy region as the itinerant s, p, and d electrons. It was shown that an overestimation of the itinerancy of 4f states leads to an unphysical large density of minority 4f states at the

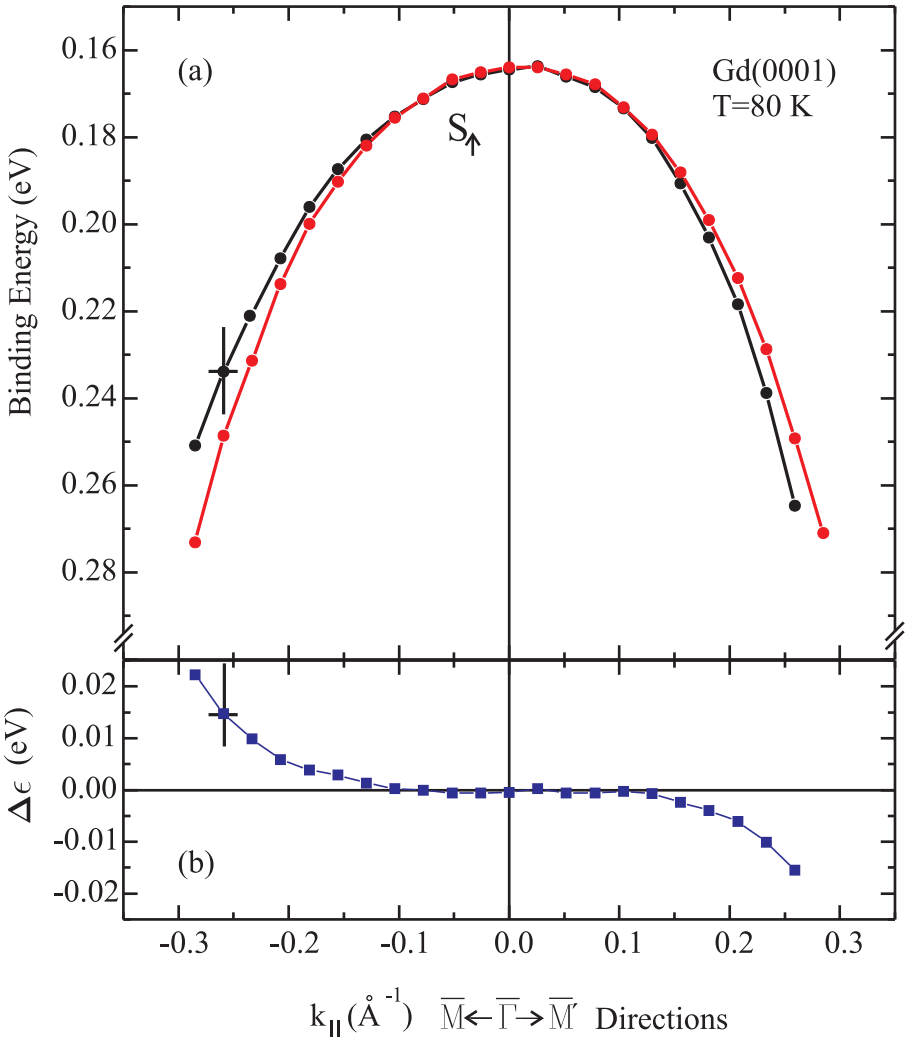

Figure 10.3: (a) Experimental results for the dispersion of the majority-spin surface state on Gd(0001) at T=20 K. Red and black filled dots correspond to opposite magnetization directions; see Fig. 3.8 for the experimental geometry. (b) Rashba spin-orbit splitting $\Delta\epsilon(k_{\|})$ derived from the data in (a). Typical error bars in (a) and (b) are given by crosses.

Fermi level; this would result in the prediction of an incorrect antiferromagnetic ground state of bulk Gd [92].

Density-functional-theory (DFT) calculation with the so-called LDA+U energy functional gives at present the most successful description of the localized 4f electrons. Within this model, the strong intra-atomic Coulomb and exchange interactions of the localized electrons are introduced and treated in a Hartree-

Fock-like manner. One effect of this model is that the occupied and unoccupied 4f states split apart, moving the minority 4f states well above the Fermi level; computational details can be found in Ref. [92].

Calculations of the gadolinium electronic structure were performed using DFT in local-density approximation (LDA) in the form of Moruzzi et al. [93]. For a proper description of the 4f electrons the LDA+U method [94] was used as described in Ref. [92]. The full-potential linearized augmented plane-wave method in film-geometry [95, 96] was applied as implemented in the *Fleur* program. Spin-orbit coupling was included self-consistently in a pseudo-perturbative manner [97]. In the calculations, the experimental value for the Gd bulk lattice constant a =6.858 au was used and the c/a ratio was kept fixed at the experimental value of 1.597 [92]. The plane-wave cut-off for the basis function was set to K_{max}=3.0 au^{-1}. The charge density and the potential were expanded up to a cut-off of G_{max}=9.0 au^{-1}. The muffin-tin radius was set to the RMT=2.80 au. The wave function as well as the density and the potential were expanded up to $l_{max} = 8$ inside the muffin-tin spheres. The Gd surface was simulated by a relaxed 10-layer film embedded in semi-infinite vacua.

The most interesting feature of the Gd(0001) electronic structure is the surface state located in the gap of the projected bulk band structure around $\overline{\Gamma}$. The energy dispersion of the occupied majority component is shown in Fig. 10.4. Both the minority and the majority part of the surface state are strongly localized at the surface. The LDA calculation shows that over 70% of its charge density is located in the surface layer and in the vacuum region, and that it has mainly 5d character inside the surface muffin-tin sphere. Hence, the interaction with the sub-surface layer, the gadolinium "substrate" is rather small. This argument is further substantiated by the very weak dependence of the surface-state binding energy (minority and majority part) on interlayer relaxation and also on the type of close-packed stacking of the surface layer (fcc vs. hcp) [70].

For the ab-initio calculations of the Gd(0001) surface including SOC, the magnetic moment was taken to be in the surface plane. Results without spin-orbit coupling were previously presented in Ref. [92]. In presence of SOC, magnetization lowers the $p3m1$ symmetry of the hcp(0001) surface to cm symmetry. Using a pseudo-hexagonal notation, we can still label the high-symmetry points of the BZ as $\overline{M}$ and $\overline{K}$, but with subscripts to distinguish between inequivalent points in the Brillouin zone, see inset of Fig. 10.4. Points that are related by an inversion center are primed to indicate that the bandstructure upon inversion is equivalent to the unprimed $k_{\|}$-points if one interchanges spin-up and spin-down bands. In the calculation, the magnetization was assumed to point in the direction of the in-plane nearest neighbors. In this case the strength of the Rashba splitting decreases from the $\overline{\Gamma} \rightarrow \overline{\mathrm{M}}_1$ direction to $\overline{\Gamma} \rightarrow \overline{\mathrm{K}}_1$ and $\overline{\Gamma} \rightarrow \overline{M}_2$, and is found to be zero in $\overline{\Gamma} \rightarrow \overline{\mathrm{K}}_2$ direction. In the calculation, the surface was simulated by a thin film having an upper and a lower surface. Since the potential gradients on these two surfaces have opposite directions, we observe for the surface state on the upper and the lower surface Rashba splittings that would result from two calculations of a surface state on one of these surfaces, but with opposite magnetizations. A comparison with Fig. 10.3 shows that the

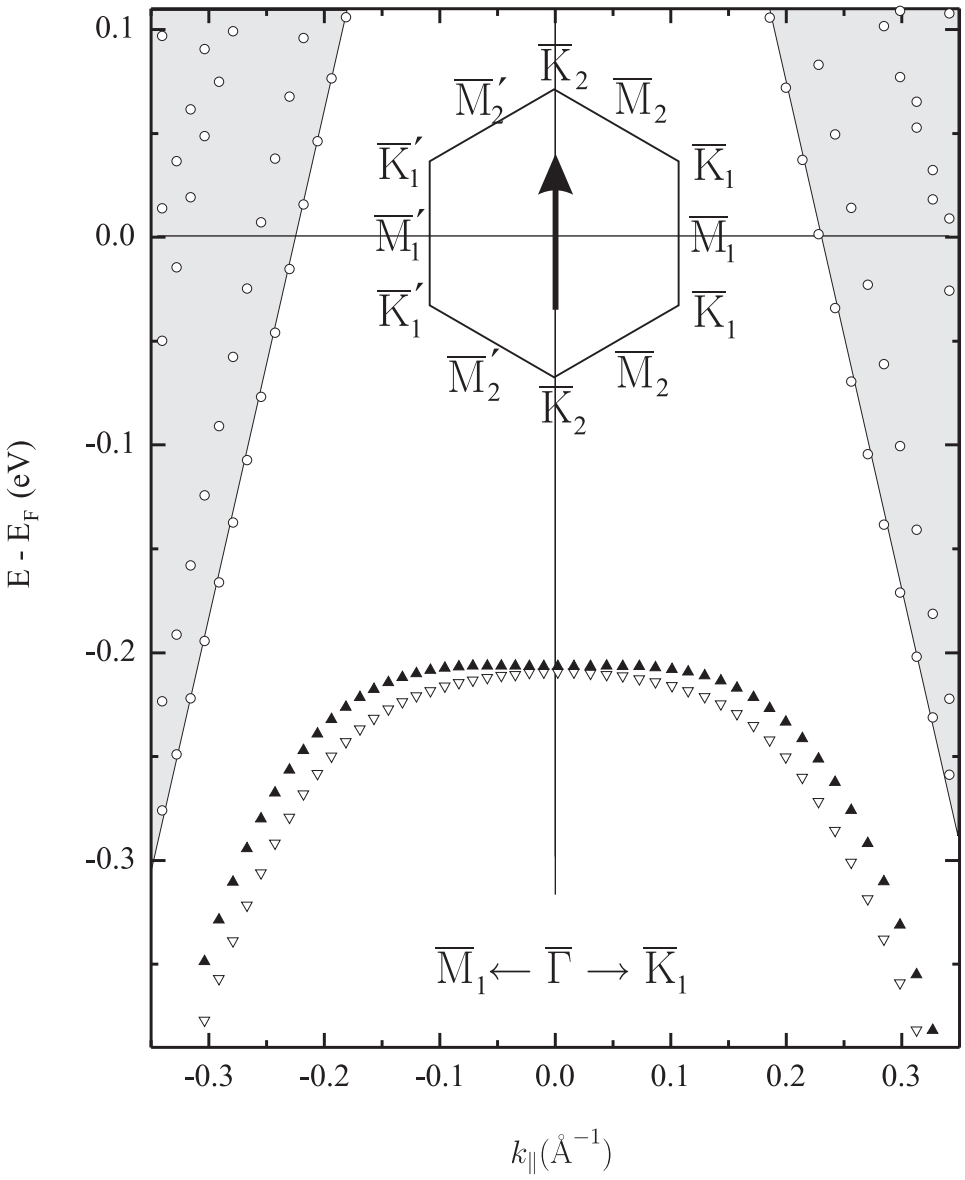

Figure 10.4: Calculated majority-spin surface-state dispersion of Gd(0001) along two high-symmetry directions of the surface BZ. There are two different dispersions for each of the two directions; they originate from the surface state on the upper surface (empty symbols) and lower surface (full symbols) of a 10-layer Gd slab; these two dispersion curves are equivalent to those of a Gd surface with two opposite magnetization directions.

calculated Rashba splitting agrees rather well with the experimental values.

To further support and complete the picture, it would be highly instructive to investigate opposite spin orientations simultaneously in one experiment, i.e.

to perform a PE experiment on a surface where both minority and majority states are located below the Fermi level; it is fortunate that such a situation can indeed be realized on the gadolinium surface by adsorption of a monolayer of oxygen [63].

10.2 The $p(1 \times 1)O/Gd(0001)$ interface

Experiment

Adsorption of oxygen on Gd(0001) leads to the formation of a $p(1\times1)O/Gd(0001)$ superstructure. It is accompanied by a strong modification of the surface electronic structure, in particular changes in energy position and dispersion of the surface state; this is shown in Fig. 10.5(a). The surface monoxide phase exhibits an exchange-split pair of surface bands that originate from hybridisation of Gd 5d and O 2p states. Both the minority and the majority band are now below the Fermi level; they exhibit an upward dispersion, with the minority band having a significantly larger curvature (corresponding to a smaller effective mass). Due to exchange interaction they have well separated binding energy minima of 0.4 eV (minority) and 0.85 eV (majority).

In close analogy to the Gd metal case, these exchange-split surface bands shift considerably with respect to the center of the Brillouin zone when the magnetization direction is reversed, see black and red filled dots in Fig.10.5(a). The shift is opposite for $S_\uparrow$ and $S_\downarrow$, in agreement with what is expected from the triple-vector product in Eq. 9.2. This behavior gives strong support to an identification of this splitting as Rashba splitting.

The energy difference $\Delta\epsilon$ between states of equal momentum but opposite spin is plotted separately for $S_\uparrow$ and $S_\downarrow$ in Fig. 10.5(b). It is considerably increased as compared to the metal case, amounting up to 100 meV ($S_\downarrow$) in the interval $\left|k_\parallel\right| < 0.4\text{Å}^{-1}$. It clearly changes in a linearly with $\mathbf{k}_\parallel$ in agreement with our expectations from the triple-vector product of the Rashba Hamiltonian (cf. Eq. 9.2).

Ab-initio calculations: O/Gd

The experimental results shall again be compared with the results of LDA+U calculations performed by G. Bihlmayer. In these calculations, O was assumed to be adsorbed at the fcc site, and its relaxed position was found to be 0.78Å above the topmost Gd layer. The outermost metal layer exhibits a strong outward relaxation (by $\simeq$18%) upon O adsorption, while the inner layers remain nearly unperturbed. Very similar results were obtained for O adsorbed on the (energetically slightly less favorable) hcp site. For the calculations a plane-wave cutoff of $k_{\max} = 3.8$ (a.u.)$^{-1}$ was used, and the irreducible part of the two-dimensional Brillouin-zone (BZ) was sampled at 21 special $\mathbf{k}_\parallel$ points. For the calculations with SOC included, 36 $\mathbf{k}_\parallel$ points were sampled.

The electronegative oxygen atoms, adsorbed at the gadolinium surface, have a strong effect on the entire near-surface charge distribution and consequently on the energy dispersion of the surface state, which is shown in Fig. 10.6. In

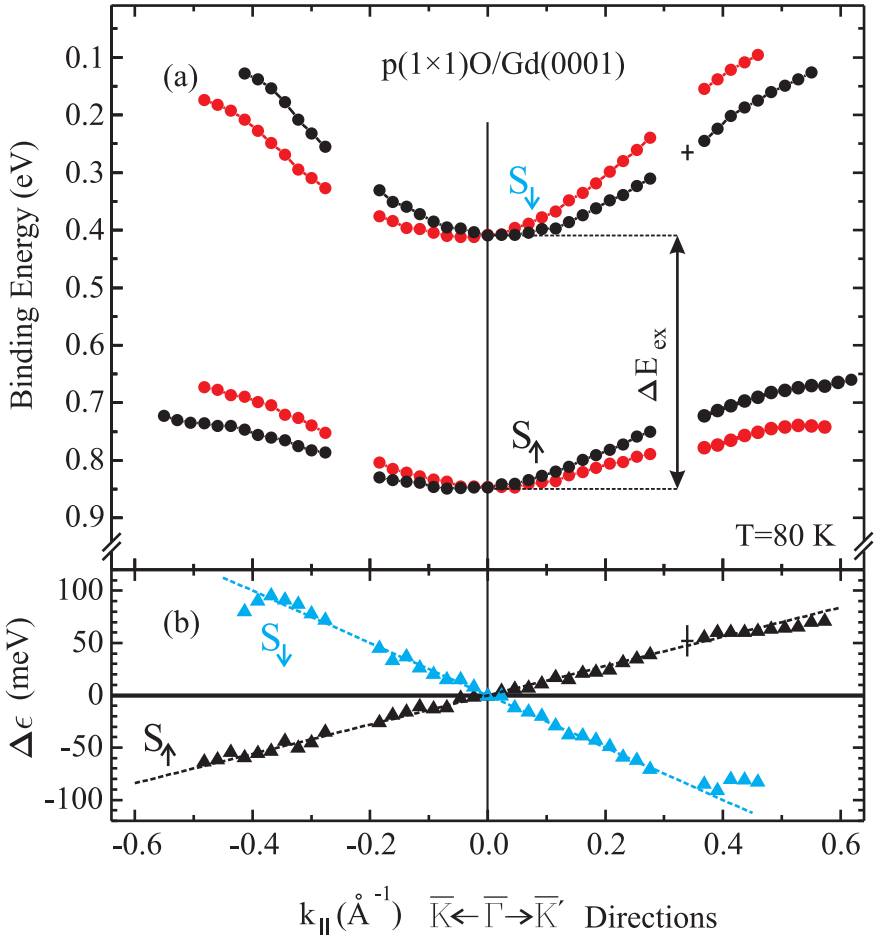

Figure 10.5: (a) Energy dispersion curves for the $S_\uparrow$ (majority) and $S_\downarrow$ (minority) surface state, respectively, in the valence-band region upon formation of the $p(1 \times 1)$O superstructure on Gd(0001). At T=80 K, $S_\uparrow$ and $S_\downarrow$ are exchange split by ΔE_{ex}=450 meV at $\overline{\Gamma}$. Red and black filled dots correspond to two positions of the energy dispersion $E(k)$ for opposite magnetization directions. (b) Rashba splitting $\Delta\epsilon(k_\parallel)$ derived from the experimental data in (a). Dashed lines represent linear fits to $\Delta\epsilon(k_\parallel)$.

good agreement with the experimental data presented in Fig. 10.5(a), we find two occupied states dispersing upwards, the minority state located at −0.5 eV relative to the Fermi level (at $\overline{\Gamma}$). The exchange splitting amounts to 0.8 eV and is some 0.35 eV larger than the experimentally observed one; a similar overestimation of the exchange splitting had previously been found in the calculations for Gd(0001) metal [92].

The Rashba splitting of the surface states is calculated to be about five times larger than that of the Gd(0001) metal surface, in good agreement with the experimental observation.

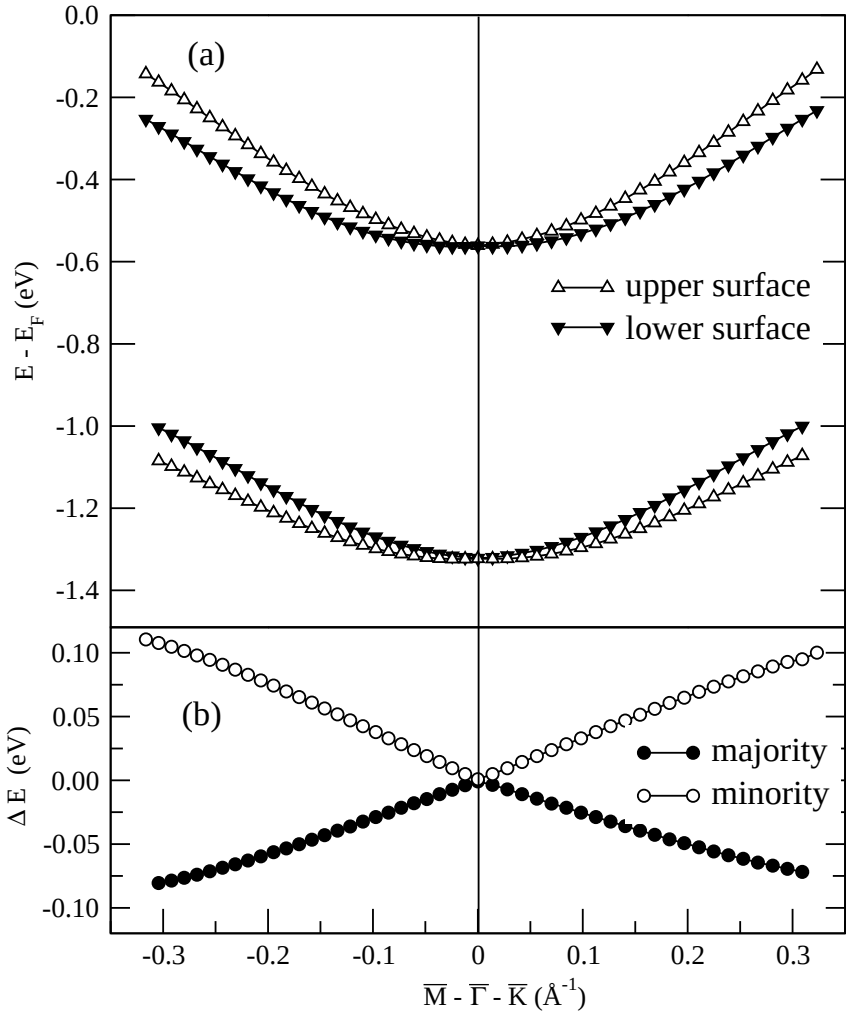

Figure 10.6: (a) Calculated surface-state dispersion for $p(1 \times 1)O/Gd(0001)$ along high symmetry directions of the surface BZ. The exchange-split bands are shifted considerably with respect to $\overline{\Gamma}$ into opposite k directions. (b) Rashba splitting $\Delta\epsilon(k_{\|})$ for majority and minority bands, calculated from the data in (a).

10.3 Density-of-states and surface-state charge distributions

It is instructive to compare the theoretically calculated DOS at the Fermi level of Gd(0001) and O/Gd(0001). Fig. 10.7 displays the layer-resolved density of states of Gd(0001), where contributions from s, p, and d electrons are shown separately. The DOS was calculated for regions inside the muffin-tin spheres of different layers of a ten-layer Gd(0001) film. The main contribution to the DOS near the Fermi level originates from d electrons. Moving from the surface layer to the subsurface, the DOS changes rapidly, resembling the bulk shape

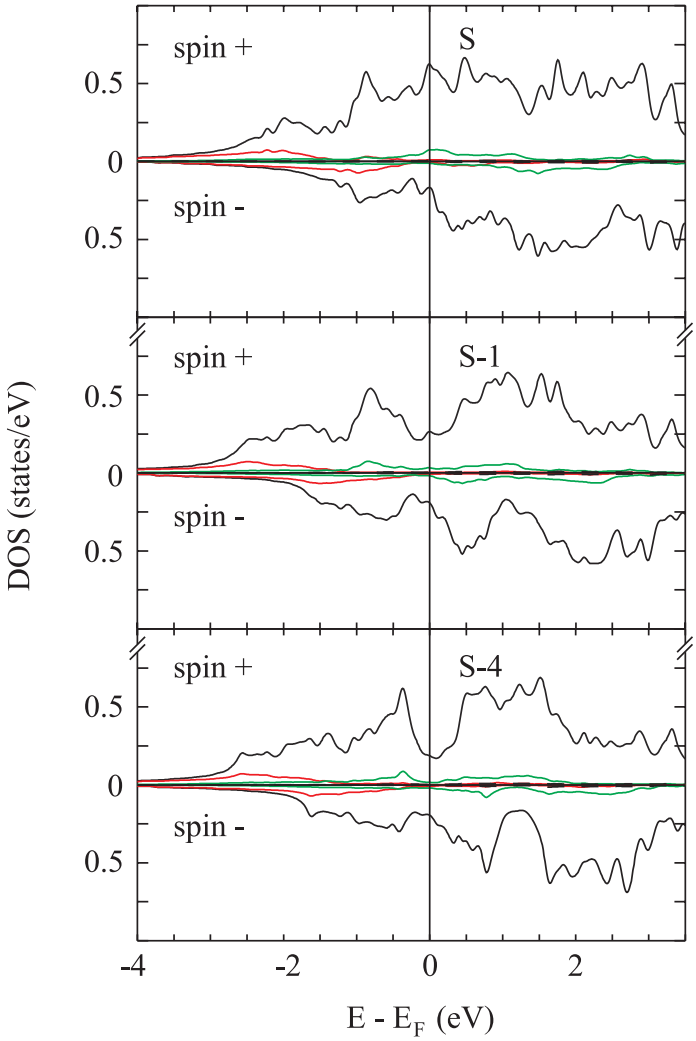

Figure 10.7: Layer- and spin-resolved DOS of gadolinium obtained from the LDA 4f-core calculations using a ten-layer Gd(0001) slab: the calculations of s (red), p (green), and d (black) electrons inside the muffin-tin spheres are shown separately for the different layers: S: surface layer; S-1: subsurface layer; S-4 represents the center of the film. From Ref. [92].

already in the subsurface layer. The majority DOS of the middle layer reveals a pronounced depression at the Fermi level, which is characteristic for the bulk DOS [92]. Its minority counterpart is located at 1.2 eV above the Fermi level due to exchange splitting. The exchange split pair of surface states falls exactly into this energy region and thus fills these depressions (they are not visible in the surface layer DOS). But already in the subsurface layer the depressions are clearly visible, supporting the notion of a rather high surface localization of the surface state.

Results of the DOS calculations for the surface monoxide system $p(1 \times 1)O/Gd(0001)$ are shown in Fig. 10.8 for comparison. The adsorbed O atom (on

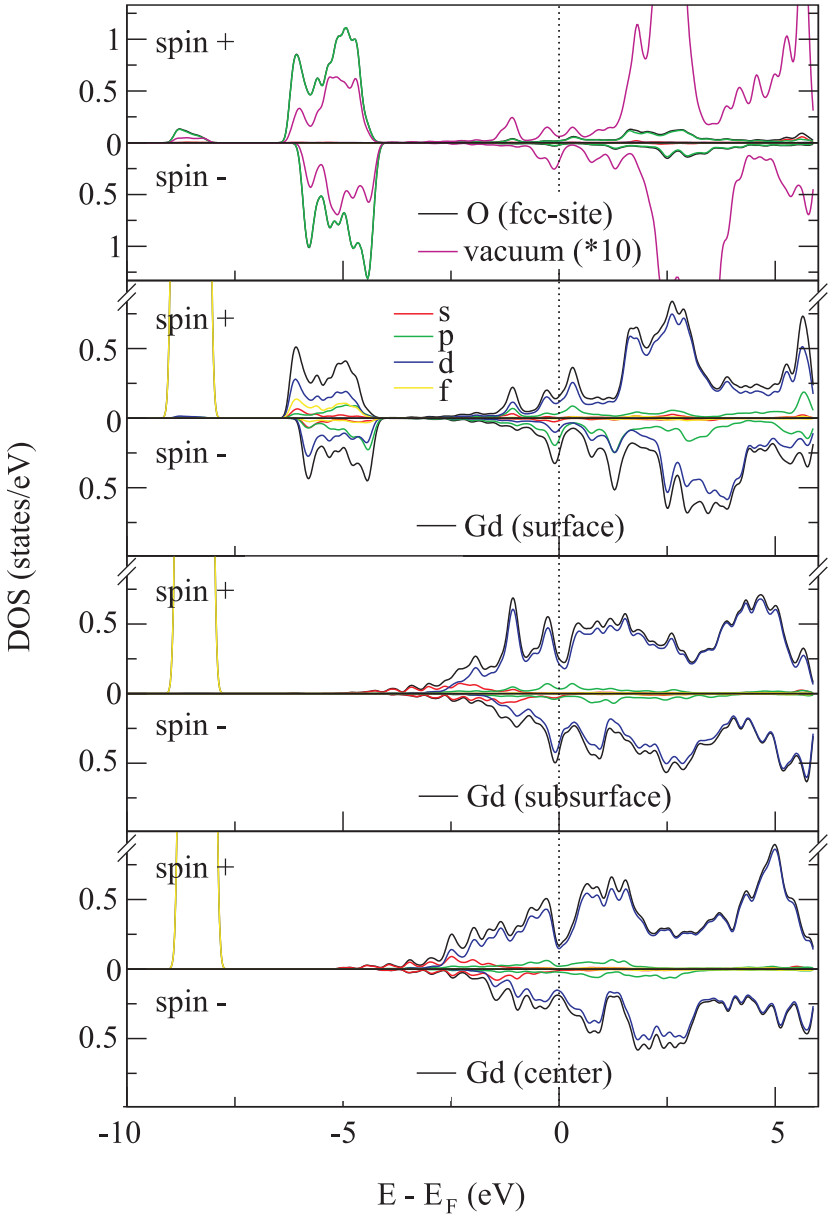

Figure 10.8: Layer- and spin-resolved DOS for $p(1 \times 1)O/Gd(0001)$ with a relaxed surface, obtained from LDA+U calculations with SOC, using a ten-layer slab. Displayed are the DOS inside the muffin-tin spheres of different layers with orbital resolution: s electrons: red; p electrons: green; d electrons: blue; f electrons: yellow.

an fcc site) strongly modifies the electronic structure of the entire near-surface region. The Gd in the surface and in the subsurface are modified, whereas the DOS of the center layer, as expected, shows no difference to the elemental gadolinium film. The strongest effects of O adsorption occur in the surface layer, where the DOS near the Fermi level is clearly reduced, and characteristic

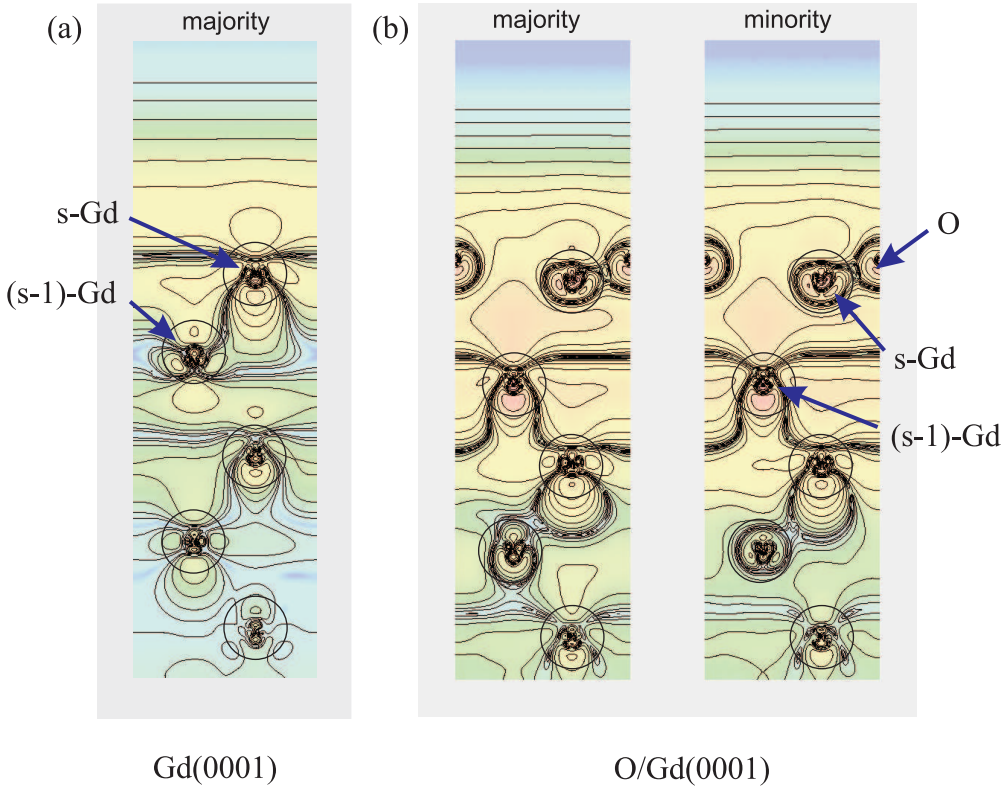

Figure 10.9: Charge-density contour plots of the majority and minority parts of the surface state in a plane perpendicular to the surface. The plot shows a cross section through half of the film cutting five atoms. Changes of charge densities are shown by color changes (log scale) from red to blue, when going from high to low densities. For $p(1 \times 1)O/Gd(0001)$, both the majority and the minority parts of the surface state are occupied. Black circles mark the muffin-tin spheres around each lattice site.

features appear at about 5-eV binding energy, indicating charge transfer from the Fermi energy region as well as O-Gd bond formation.

Fig. 10.8 also shows that – upon oxide-layer formation – there is a redistribution of the orbital characters of states near the $\overline{\Gamma}$-point inside the gadolinium muffin-tin sphere. The orbital character changes from almost purely d-like to a substantial admixture of p character (as well as minor s contributions). In particular, the p contribution even exceeds the d-contribution in the minority part of the surface-layer DOS below the Fermi level.

The relative weights of electrons with different orbital character in the first layer (inside the muffin-tin spheres) change from s:p:d = 0 %:3 %:23 % for elemental Gd(0001) to 6 %:20 %:2 % for $p(1 \times 1)O/Gd(0001)$. In the second layer these weights change from s:p:d = 0 %:0 %:2 % to 2 %:3 %:14 %. The rest of the electron charge density is mainly in the interstitial and vacuum regions.

In agreement with the results of resonant PE experiments [63], the calculations indicate strong oxygen contributions to the oxygen-derived states.

Figure 10.9(a) displays charge-density profiles of the occupied majority-spin surface states of the Gd(0001) surface. The shapes of the charge-density contour lines clearly reveal the d_{z^2}-symmetry of the surface state (s-Gd). The strong surface localization is quite remarkable, also the large fraction of the surface state that extends into the vacuum region.

The electronic charge distribution changes considerably upon oxygen adsorption, see Fig. 10.9(b). The characteristic charge contours of the majority and minority parts of the surface state for $p(1 \times 1)O/Gd(0001)$ resides no longer in the s-Gd layer, as it does for the metal surface, but has shifted to the subsurface layer, (s-1)-Gd. As a consequence, this state should rather be considered *an interface state* between bulk Gd metal and the surface monoxide $p(1 \times 1)O/Gd(0001)$ layer. Also, most of the charge density in the vacuum region (amounting to 40 % in case of Gd(0001) is drawn towards the surface layer and below (only 6 % remain in the vacuum region).

The changes in charge-density contours of the surface state are remarkable. The comparison of the clean and oxidized gadolinium surfaces reveals that the character of the "surface state" has changed considerably upon oxygen adsorption: on Gd (0001), it resembles the symmetrical shape of a d_{z^2}- orbital, while upon oxidation the state has become rather asymmetric.

10.4 Modification of Rashba interaction through oxidation

The observation of an increase of the Rashba splitting through oxygen adsorption on the Gd(0001) surface raises the question about its origin, and about the underlying microscopic mechanism. In an attempt to answer this question, we benefit from our discussion of model cases in Chapter 9. The observed changes can be appreciated particularly well by comparing with the results of the tight-binding model that allows to identify the main contributions to a sizeable Rashba effect at the surface, in addition to the gradient of the surface potential: these are the atomic spin-orbit interaction and the orbital characters of the wave functions involved.

Atomic SOC

The layer-resolved Rashba spin-orbit contributions to the total splitting are plotted in Fig. 10.10. One can see that, in case of the clean Gd(0001) surface, the first layer provides the main contribution of the total splitting; already the second layer contributes less than 10 %. In the surface-monoxide case, the situation changes dramatically, since the main contribution to the splitting arises from the subsurface (S-1) layer, whereas the first and third layer contributes only 18 % and 10 %, respectively. These numbers correspond well to the changes in the occupation of the muffin-tin spheres around the atoms at these surfaces. When summing up the partial charge contributions from s, p, and d orbitals to the surface state within the muffin-tin spheres (cf. Fig. 10.9), they increase upon oxygen adsorption from 26 % to 28 % in the S layer and from 2 % to 19

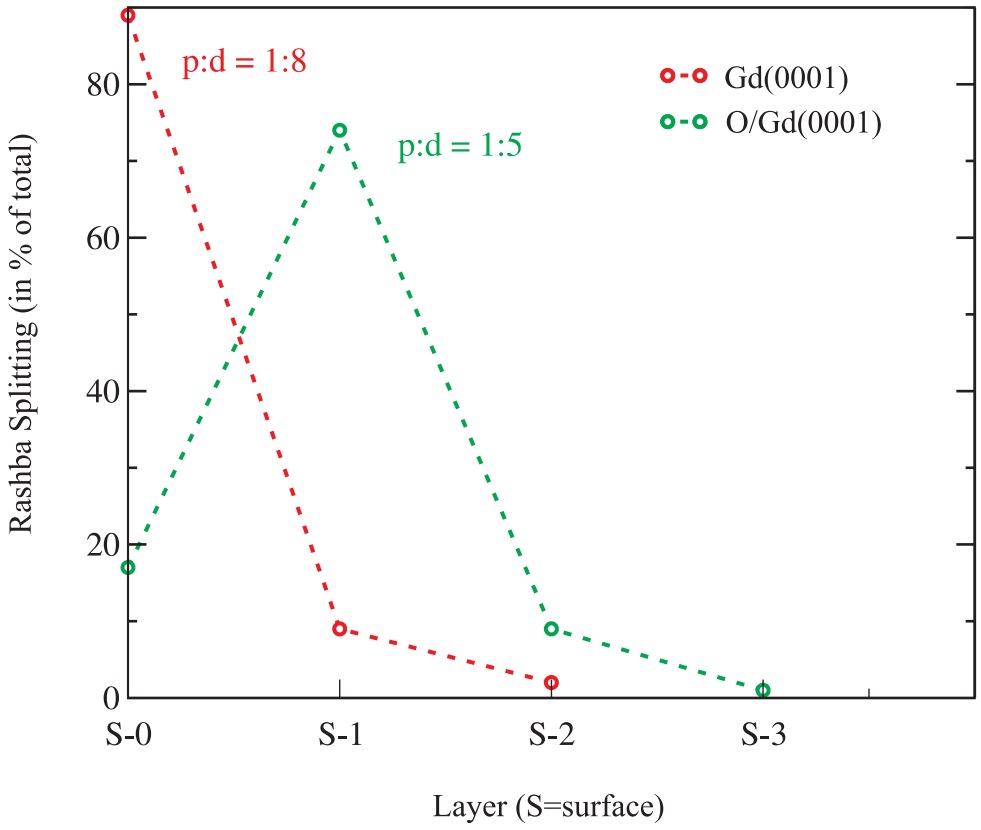

Figure 10.10: Contributions of individual layers to the Rashba splitting for Gd(0001) and $p(1 \times 1)O/Gd(0001)$ in the near-surface region (dashed lines are guide for the eyes). The p:d ratios are the relative weights of p and d states in these layers, which give the maximum contributions to the Rashba splitting in each case.

% in the (S-1) Gd layer. This results in an increase of electronic charge by 70 % in the regions of the muffin-tin spheres around the gadolinium atoms, which should lead to an increase of the atomic spin-orbit coupling constant by the same amount (in first approximation, with all other parameters being equal).

For the surface monoxide structure, the contribution of p states is enhanced as compared to the clean gadolinium surface (cf. Fig. 10.10). In a free atom, the spin-orbit splitting of electronic levels is well known and can be described by $H_{SOC} = \frac{Z_{eff}^4}{n^3}\frac{1}{l(l+1)}$. The factor $\frac{Z_{eff}^4}{n^3}$ can be estimated for the gadolinium atom, but it is difficult to use this expression for describing changes due to bonding between oxygen and gadolinium. However, using this expression we estimate the effect of p-state admixture to a spin-orbit split d state: 1/l(l+1) changes from 1/6 to 1/2 when going from a pure d to a pure p state. This would lead to an increase of the Rashba splitting by a factor of 3 (in our rather crude central-potential picture).

Also, one can calculate the matrix element of the spin-orbit-interaction

Hamiltonian $\langle \psi \left| \frac{1}{r}\frac{dV}{dr} \right| \psi \rangle$ using $V(r)$ as calculated for the gadolinium atom, and the electronic wave function corresponding to the surface state as calculated either for the clean Gd metal surface or the oxidized surface. This estimate predicts an increase of the atomic Rashba constant by a factor of 20 for the oxidized Gd surface as compared to the clean one. This qualitative result can be added to the previous arguments that tried to explain the increase of the Rashba interaction strength upon oxygen adsorption.

Still, this is only a qualitative argument. In the free atom, the value of the spin-orbit splitting is defined by the gradient of the spherical potential. It is significantly modified in the valence-band region of a solid, where the shape of the radial wave function deviates from the atomic case and itinerant electrons contribute to the screening of the nuclear charge. Let us compare with the noble-metal case, where the atomic $p_{3/2} - p_{1/2}$ splitting is 470, 110, and 31 meV for Au, Ag, and Cu, respectively. For the gold surface state, the Rashba splitting is only 110 meV [82]. If only the atomic spin-orbit interaction would be relevant, one would expect a splitting 26 and 7 meV for the silver and copper surface state, respectively; the latter splittings have been found to be negligibly small [25].

The potential gradient within the muffin-tin sphere around a Gd atom increases as well, pointing to an enhanced atomic contribution. However, changes in the potential gradient do not necessarily lead to changes in SOC in a simple way, as one can see again at the example of the noble metals. Expanding the potential gradient in spherical harmonics within the atomic spheres of Au and Ag surface atoms results in very similar coefficients for the Y_1^0 term of -0.08 and -0.07, respectively. Nevertheless, the Rashba splitting of the surface state is visible only for the gold surface, with a maximum value of 110 meV at the Fermi level (compared to 2 meV a theoretically predicted for the silver surface). It is rather difficult to understand such a drastic difference for these rather similar sp-like surface states. An explanation could be the admixture of d_{z^2} states to the gold sp-like surface state, leading to a more effective spin-orbit coupling. This had been illustrated before on the basis of the tight binding model [83].

Orbital character

Besides atomic SOC, the asymmetry of the electronic charge distribution of the surface state is an important condition for the Rashba effect to occur, and it can serve as a sensor for the effective coupling between Rashba and atomic SOC terms. We shall elucidate this in the following. In the tight-binding model, the condition of inversion-symmetry breaking leads to the admixture of a p_z state (representing the surface state) to the given p_x, p_y band. The resulting asymmetrical charge distribution of the electron cloud with respect to x, y plane (see Fig. 10.11) results in a non-zero overlap matrix element (hopping parameter) between p_z and p_x, p_y orbitals. We note here that without broken inversion symmetry the inversion $z \rightarrow -z$ would lead to an equally large overlap of the p_x, p_y orbitals with the positive and negative lobe of p_z, with the result that the hopping parameter would vanish. One can use this result of the tight-binding model as a qualitative argument when discussing real systems.

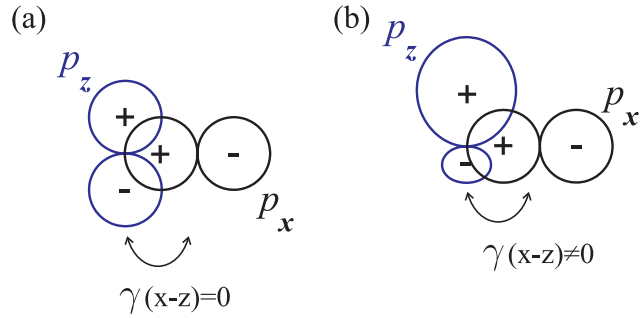

Figure 10.11: Modification of the p_z orbital by the influence of an electric field, leading to a non-equal overlap of the p_x, p_y orbital lobes with the positive and negative lobes of the p_z orbital; this results in non-zero hopping parameters between p_z and p_x, p_y orbitals: (a) zero electric field ($\gamma = 0$); (b) non-zero electric field ($\gamma \neq 0$).

The importance of the shape of the wave function has also been shown in a recent LDA+U calculation for the surface state on Lu(0001); the results of this work are reproduced in Fig. 10.12 (see Ref. [98]). It shows that at different points of the surface BZ there is a different symmetry of the surface state. The charge distribution at the $\overline{\Gamma}$ point is practically symmetric while it is strongly deformed at the $\overline{M}$ point; the corresponding band structure shows no splitting at $\overline{\Gamma}$ and a sizable effect at the $\overline{M}$ point. This provides further support for the connection between the shape of an electronic wave function and the magnitude of the Rashba splitting.

In good agreement with our observation of an increased Rashba splitting of the surface state caused by oxygen adsorption, Fig. 10.9 reveals a strong deformation of the electronic cloud at the $\overline{\Gamma}$ point for $p(1 \times 1)O/Gd(0001)$ (for the minority and majority part) but practically a symmetric distribution for the majority surface state on the clean surface. All these examples allow us to state that the shape of the electronic charge cloud is an important parameter for the Rashba effect, which can be used for qualitative arguments.

10.5 Fermi surfaces modified by Rashba interaction

The Rashba spin-orbit splitting of the exchange-split surface state at the magnetic surface of gadolinium metal reveals an essential difference to the splitting of states on non-magnetic surfaces studied before. Our comparative analysis is illustrated by the sketches given in Fig. 10.13. The upper row displays Fermi surfaces for the different cases, while the middle and the lower rows give the associated energy dispersions in two perpendicular directions (k_x and k_y direction). For the magnetic surfaces, the magnetization was assumed to be parallel to the k_y direction.

Fig. 10.13(a) presents a schematics of the Rashba spin-orbit splitting of a nonmagnetic surface. In this case, the surface state has a large in-plane spin

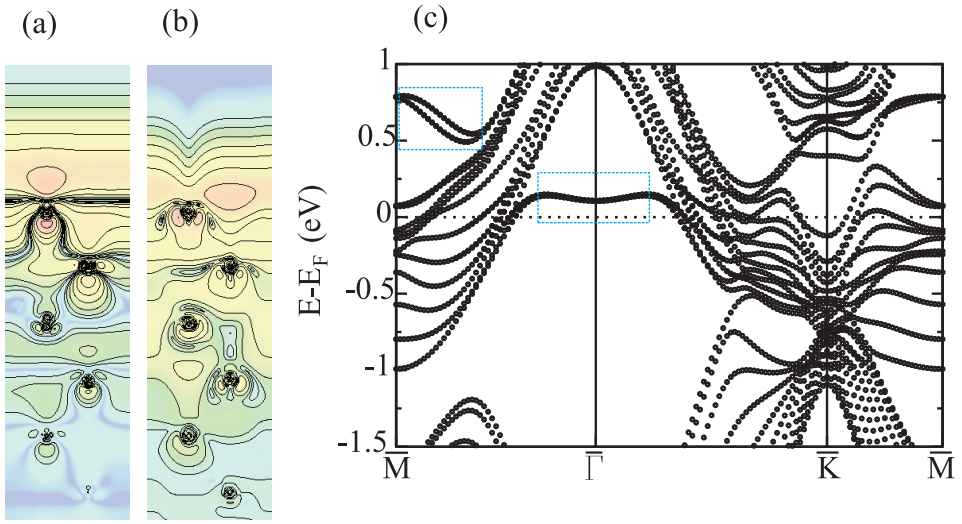

Figure 10.12: (a,b) Comparison of the electronic charge-density distributions of the unoccupied surface state on Lu(0001) at (a) the $\overline{\Gamma}$ point and (b) the $\overline{M}$ point of the surface BZ as calculated by DFT in LDA+U. The logarithm of the charge density is displayed for half of a relaxed 11-layer slab; the density changes by half an order of magnitude from one isoline to the next. (c) Calculated band structure of the Lu(0001) film (from Ref. [98]).

polarization, which remains always perpendicular to the electron propagation direction and to the electric field. This case was discussed previously using the two-dimensional free-electron gas as an example (see Sect. 9.1). The Rashba-split states have opposite spin polarization that rotates clockwise or counter-clockwise around the origin. The net spin polarization at the surface is evidently zero, and the system remains non-magnetic.

In systems with spontaneous magnetic order, the exchange interaction can be much larger than the spin-orbit interaction, as is seen, for example, when comparing the values of exchange-splitting and Rashba splitting for the case of gadolinium metal and of O/Gd. Therefore, the spin orientation is defined by the exchange interaction, and all spins are macroscopically aligned along one axis. This difference in spin structure in the surface is illustrated in the upper row of Fig. 10.13, cases (b) and (c). In the center column (b) we consider the hypothetical case of a magnetic surface without magnetic exchange splitting. There is also a significant difference in the Fermi-surface contours with regard to a nonmagnetic surface like that of Au(111), where the surface bands are split equally along all $k_{||}$ directions (see Fig. 10.13(a)), and the Fermi surfaces of a Rashba-split surface state that closely resemble concentric rings. Yet at a magnetically ordered surface, the Fermi-surface contours contain two intersecting rings of opposite spins (see Fig. 10.13(b, c)). Without exchange interaction, the rings would have the same sizes (Fig.10.13(b)). Intersection of the rings results from the Rashba Hamiltonian that is linear in the k wave vector and a fixed spin orientation (magnetization direction); this behavior is obvious from

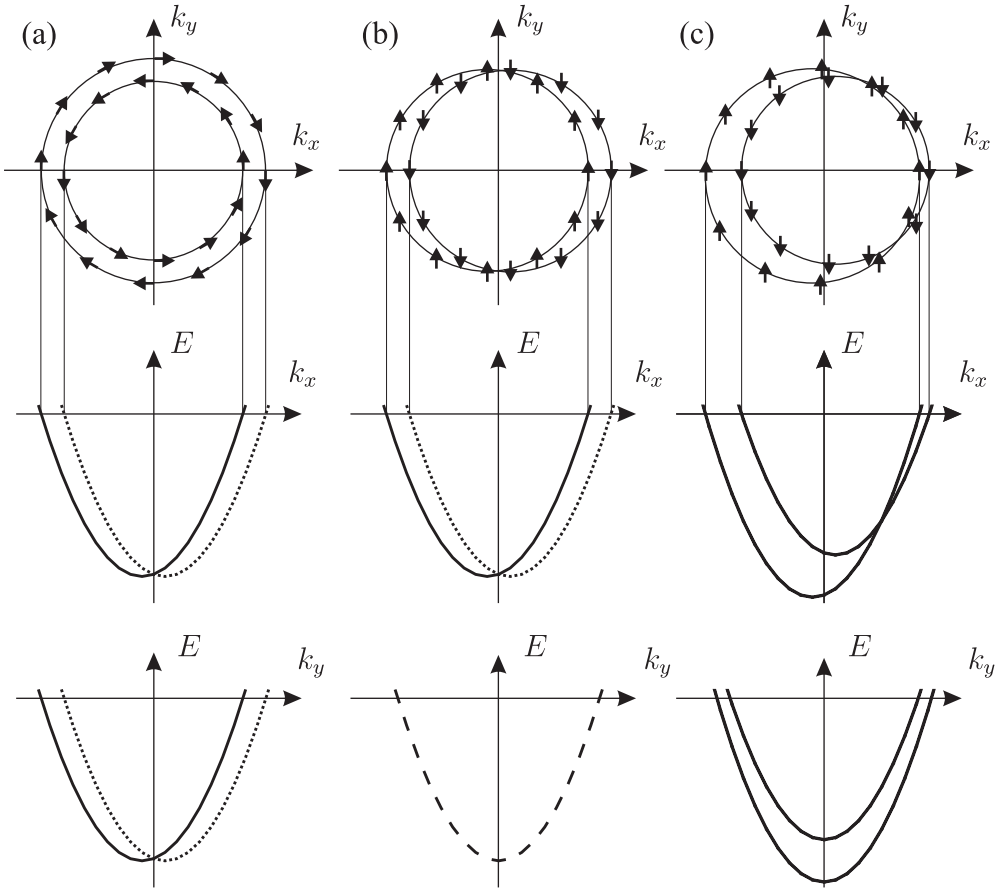

Figure 10.13: Rashba spin-orbit splitting of (a) a nonmagnetic surface, (b) a hypothetical magnetic surface without exchange splitting , and (c) a magnetic surface with exchange splitting. The upper row shows the Fermi surfaces, the middle and the lower rows display the corresponding energy dispersion curves.

the triple-vector product in Eq. 9.2. Yet, in real magnetic systems the energy bands are split by magnetic exchange interaction, which results in the situation given in Fig. 10.13(c).

It is important to note that the split bands belong to pure spin states. Therefore one has to realise that e.g. in the cases of gadolinium and terbium metal, one cannot expect to simultaneously observe a Rashba-split pair of states, as it would be tempting to do in analogy to the gold case. Because the surface states in the former cases are already split by magnetic exchange interaction, i.e. the spin degeneracy is already removed, the bands cannot split further.

The effects of a magnetization reversal are illustrated in Fig. 10.14 for the case of a magnetic surface with magnetic exchange splitting and Rashba interaction. Reversal of magnetization gives the mirror images of Fermi surface and energy dispersion curves, shown by red color in Fig. 10.14.

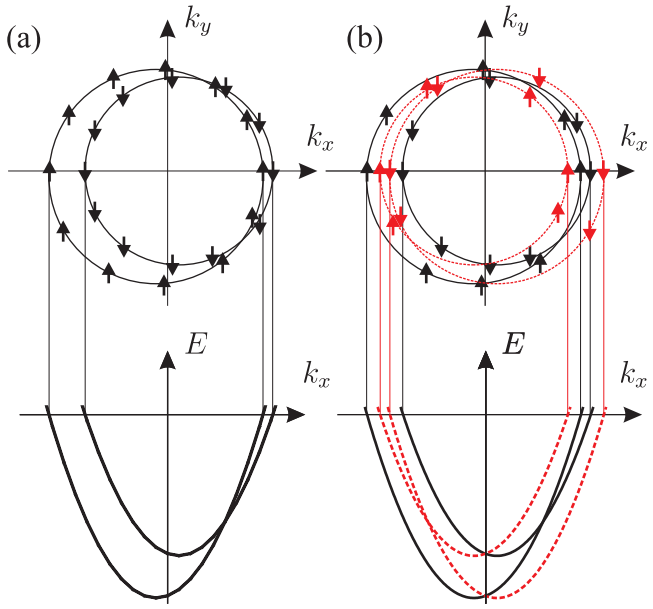

Figure 10.14: (a) Fermi surfaces and energy dispersion curves (perpendicular to the magnetization direction) corresponding to a magnetic surface that is magnetized in k_y direction; (b) Effect of magnetization reversal on a pair of exchange-split bands with Rashba splitting. The dispersion curves change from black to red upon magnetization reversal.

10.6 The Tb(0001) surface

In context of the observation of a sizable Rashba effect at the gadolinium metal surface, one should expect to find the Rashba effect at many other rare-earth metal surfaces. To test this prediction we have studied the terbium metal surface state. In comparison to gadolinium, terbium has one additional electron if the 4f shell leading to large orbital angular momentum. This renders a calculation of the band structure of Tb considerably more complicated than that of gadolinium. Nevertheless, from the experimental point of view Tb(0001) is a nicer system to study, due to the higher stability of Tb films upon annealing. This allows to prepare thin films of better quality (also surface monoxides structures).

The electronic structure in the valence-band region of the Tb(0001) surface is presented in Fig. 10.15 by a set of EDCs recorded with a constant angular shift of 0.55 degrees between the spectra. The angle-resolved PE spectra were recoded with 36-eV photon energy at a sample temperature of 80 K , where Tb is in the ferromagnetic phase. The observed electronic structure is quite typical for heavy rare-earth metals. In analogy to gadolinium (see e.g. Fig. 10.1), the surface state and T_4 band are exchange split at 80 K. Only the majority part of the surface state, $S_\uparrow$, is occupied, whereas the minority part is located above the Fermi level and can hence not be observed in a PE experiment. The surface state is rather stationary in energy near the $\overline{\Gamma}$ point, and shows a downward

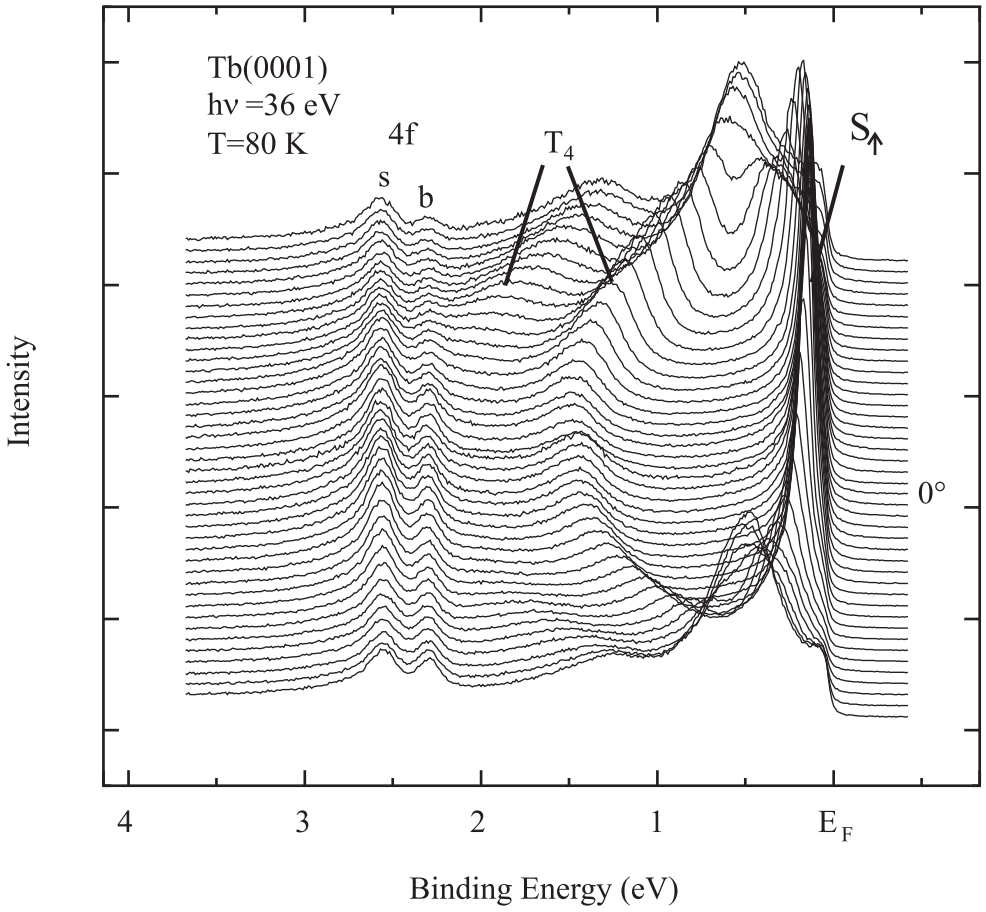

Figure 10.15: (a) Set of EDCs recorded in the valence-band region of the Tb(0001) surface with 36-eV photons and with angular steps of 0.55° between consecutive spectra. Similar to Gd(0001), the majority part of the surface state and the exchange-split T_4 band were observed. Unlike the case of Gd, the shallowest 4f multiplet component, split into surface and bulk features, is also visible around a binding energy of 2.5 eV.

dispersion (from the Fermi level) off the $\overline{\Gamma}$ point in $\overline{\Gamma} \rightarrow \overline{\mathrm{K}}$ direction. The T_4 band displays a much stronger upward dispersion, which can be used to determine the energy of the $\overline{\Gamma}$ point (band minimum). Different from the Gd case, the high-spin 4f component of the final-state multiplet of Tb splits into a surface and a bulk component and appears also in the valence-band region [60]. The observed shift of the surface component with respect to the bulk component is due to the well-known surface core-level shift that is associated with different coordination numbers of Tb atoms at the surface and in the bulk, respectively.

The effects of a magnetization reversal on the dispersion of the Tb(0001) surface state are illustrated in Fig. 10.16. The pairs of spectra recorded at normal emission and at an electron-emission angle of 2.75° (w.r.t. the surface

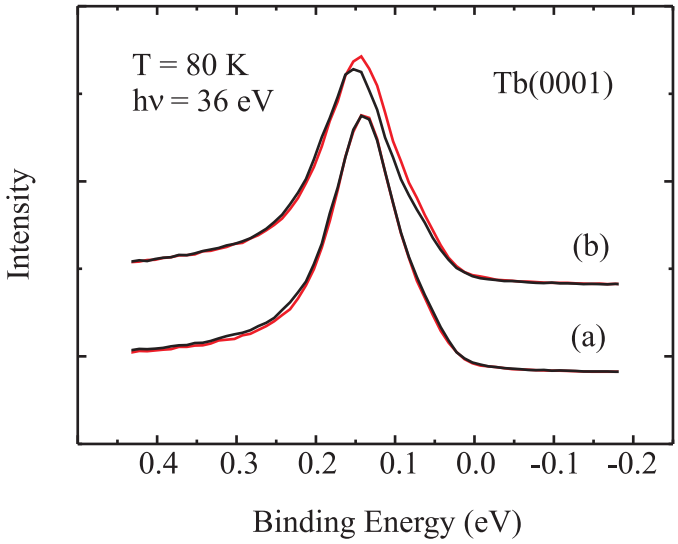

Figure 10.16: The Rashba effect upon magnetization reversal on the Tb(0001) surface causes a shift of the peak position (red and black curves) in the off-normal PE spectra: (a) 0° (normal emission), (b) 2.75°.

normal) for opposite magnetization directions reveal that the peak position of the surface state for off-normal emission depends on the magnetization, whereas there is no change for normal emission. Similar to the Gd case described above, this behavior is in agreement with what one expects from the Rashba spin-orbit Hamiltonian (see Eq. 9.2). We are not aware of any other effect besides spin-orbit interaction that could cause such a behavior.

The systematic mapping of this effect for the $\overline{\Gamma} \rightarrow \overline{\mathrm{K}}$ direction reveals the dispersive behavior shown in Fig. 10.17, with a distinctly different dispersion for the two opposite magnetization directions. The overall behavior of the dispersion of the terbium surface state is quite similar to the gadolinium case. A closer look, however, reveals differences in some details; there are additional features, which are very interesting from a fundamental point of view. In particular, there are rather linear regions of the dispersion curves near the $\overline{\Gamma}$ point (Fig. 10.17(a)), which is a manifestation of the fact that the surface states on the close-packed surfaces of rare-earth metals are derived from d_{z^2} atomic orbitals, i.e. they are rather localized valence states (with a narrow band width).

From the well-known case of Au(111) it has become customary to regard the Rashba splitting as a shift of the E($k_{\|}$) dispersion in $k_{\|}$ direction. Yet, as it becomes evident from the Hamiltonian Eq. 9.2 given in Chapter 9, the Rashba spin-orbit interaction term is an energy correction. It is not possible to match the dispersions in Fig. 10.17 by shifting in $k_{\|}$-direction. They are rather symmetric with respect to a mirror reflection at the $\overline{\Gamma}$ point, i.e. when the $\overline{\Gamma} \rightarrow \overline{\mathrm{K}}$ and $\overline{\Gamma} \rightarrow \overline{\mathrm{K}}'$ directions are interchanged.

The energy difference between the two dispersion curves (at the same $k_{\|}$

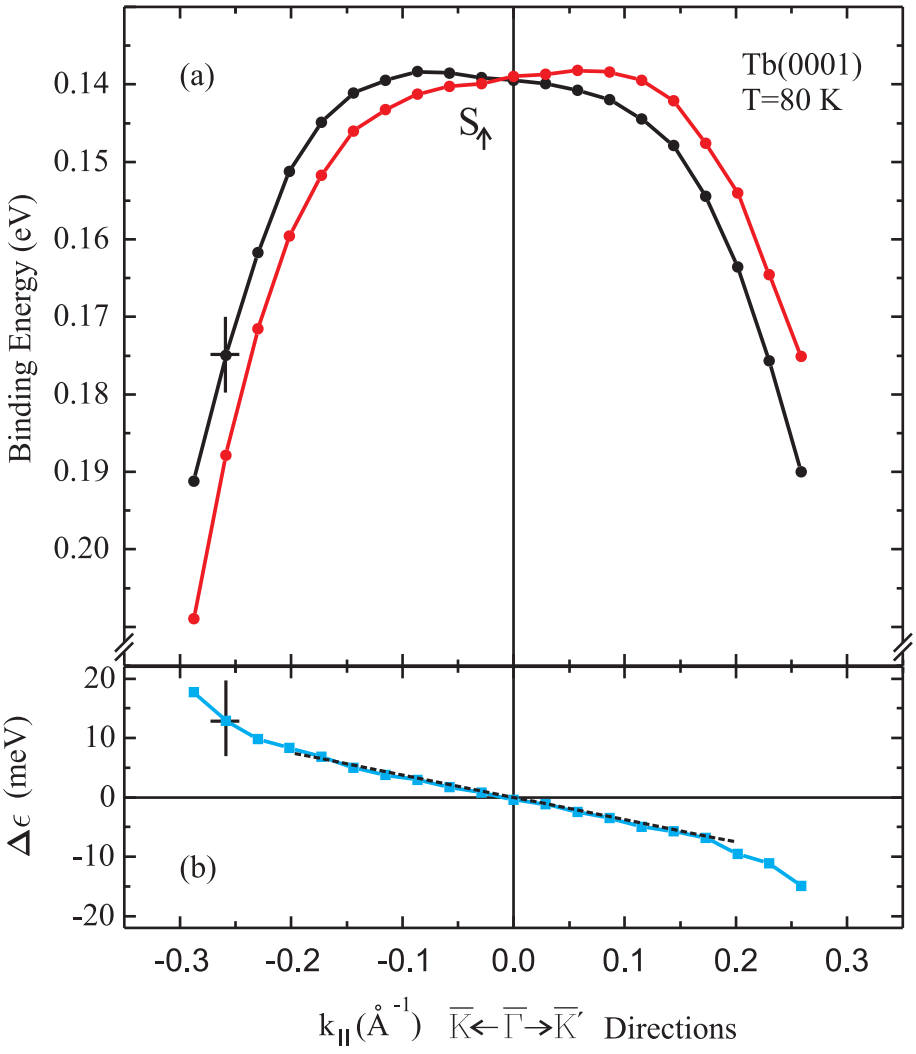

Figure 10.17: (a) Surface-state dispersion of Tb(0001) at 80 K for two opposite in-plane magnetization directions (red and black curves). (b) Energy difference between the dispersion curves in (a), together with a linear fit to the data around $\overline{\Gamma}$ (dashed line).

value) is plotted on the bottom panel (b) in Fig. 10.17; it reflects a linear behavior in the vicinity of the $\overline{\Gamma}$ point.

The calculated surface-state dispersion of Tb(0001) is plotted in Fig. 10.18. Obviously, there are deviations in some details when one compares these theoretical curves with the experimental results gives in Fig. 10.17. The flat region of the surface-state dispersion, which is visible in the experimental data, does not exist in the calculations. A likely reason is a difference in surface relaxation, which was found to have a considerable influence on the surface-state dispersion, in particular on the curvature of the dispersion near $\overline{\Gamma}$ [70]. The

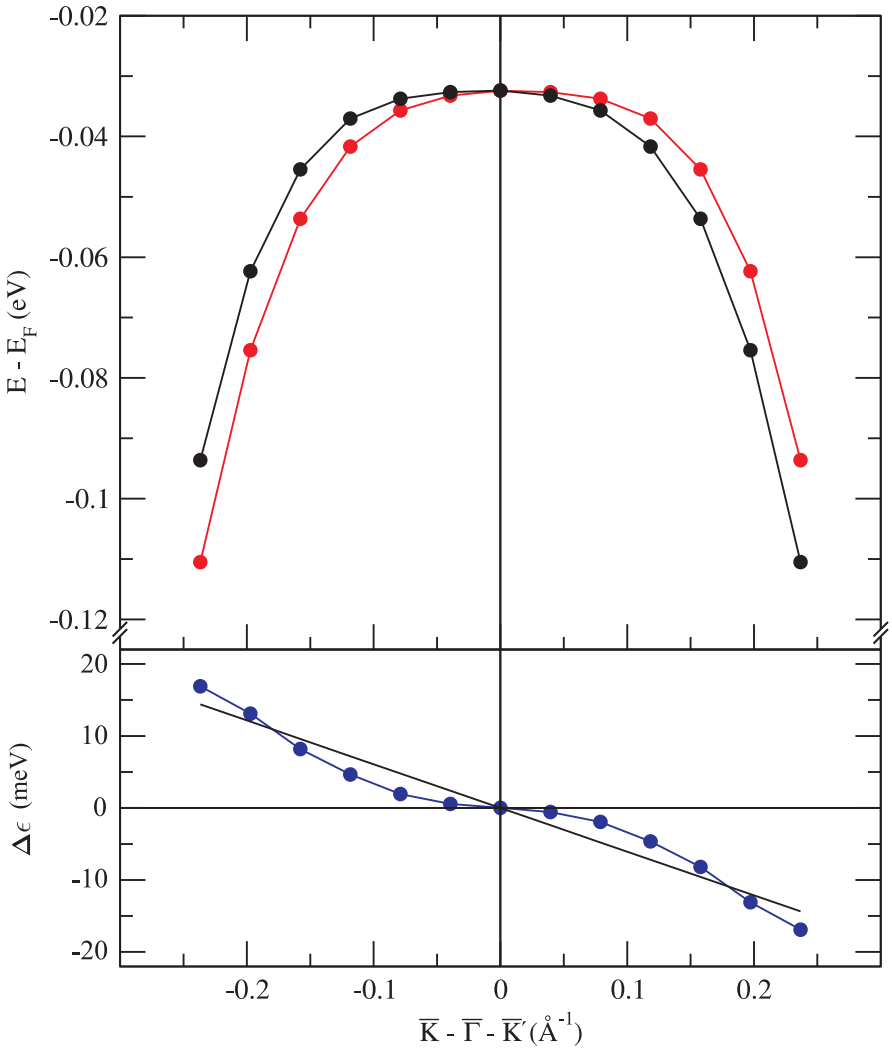

Figure 10.18: (a) Theoretical dispersion of the Tb(0001) surface state along $\overline{\mathrm{K}} \leftarrow \overline{\Gamma} \rightarrow \overline{\mathrm{K}}'$, from LDA+U calculations. The two branches (red and black) correspond to opposite magnetization directions. (b) The resulting Rashba splitting is the difference between the dispersion curves for a given $k_{\|}$ value.

qualitative agreement with experiment, however, is quite convincing.

Extended calculations for gadolinium and terbium metal (by G. Bihlmayer; not shown here) predict that the splitting increases only around the center of the BZ, before it saturates and then decreases when approaching the bulk bands at the border of the projected band gap. This non-monotonic Rashba splitting can qualitatively be understood as a consequence of the theoretically expected change of the surface state which has a varying degree of localization. It starts d_{z^2} like at the center of Brillouin zone, becoming more delocalized for larger $k_{\|}$ when the band-gap boundaries are approached. In this way, the rare-earth surface states are fundamentally different from a 2D free-electron gas.

One would expect a systematic development of the dispersion near the $\overline{\Gamma}$ point over the series of rare-earth metals from La to Lu. In the vicinity of the $\overline{\Gamma}$ point, lanthanum (similar to gadolinium) shows a clear downward dispersion (negative second derivative) whereas the surface state on Lu(0001) displays an upward dispersion (positive second derivative). When varying the interlayer distance between the first and the second layer in the LDA calculations, one realizes that the curvature of the dispersion at $\overline{\Gamma}$ reacts very sensitively. Consequently, surface relaxation can be responsible for the observed difference between the gadolinium and terbium cases.

10.7 The $p(1 \times 1)O/Tb(0001)$ interface

As for the Gd(0001) surface, a metal/metal-oxide interface can also be formed by adsorption of oxygen on the Tb(0001) surface. The $p(1\times1)O/Gd(0001)$ case served as an "ideal experiment" providing direct evidence for the connection between the spin of the propagating electron and the resulting modification in its dispersion by the Rashba effect. The valence-band electronic structure of the $p(1 \times 1)O/Tb(0001)$ overlayer is shown in Fig. 10.19 by a set of EDCs, recorded for two opposite magnetization directions with 45-eV photons and angular steps of 0.55° between consecutive spectra. The better thermal stability of the terbium surface monoxide system allows the application of higher annealing temperatures (up to 390 K) that leed to a better-ordered structure, as judged from the LEED images (compared with those of the corresponding Gd surface-oxide phase). This property renders terbium metal and its surface monoxide more favorable choices than gadolinium from an experimental point of view.

Owing to the rather big effect, the Rashba spin-orbit interaction is already clearly visible from the raw data shown in Fig. 10.19. At $\overline{\Gamma}$, the positions of the exchange-split oxygen-induced surface-state peaks do not change with the direction of magnetization; this however, is not the case for off-normal emission. For the two branches, the shifts in energy have opposite direction. Pairs of spectra are symmetrical about the $\overline{\Gamma}$ point with respect to interchange; also a sign change of the k vector has the same effect (indicated by a color change in the pairs corresponding to symmetrical k values).

Figure 10.20 displays the dispersion of the surface state on $p(1\times1)O/Tb(0001)$ along the $\overline{K}-\overline{\Gamma}-\overline{K}'$ direction, as derived from the experimental data. It is in fact quite similar to the dispersion of the states at $p(1 \times 1)O/Gd(0001)$.

The dispersion of both parts of the exchange split surface state of terbium is obviously spin dependent (see Fig. 10.20(a)). Both branches have upward dispersion, for the minority state ($S_\downarrow$) the dispersion is slightly stronger, similar to the case of gadolinium. However, in case of terbium the derived values of the Rashba splitting of the majority and the minority state are obviously the same (modulo sign) (see Fig. 10.20(b)). This shows that there is no connection between the character of the dispersion (fast vs. slow) and the value of the local splitting.

The observation of a Rashba effect on the Gd(0001) and Tb(0001) surfaces

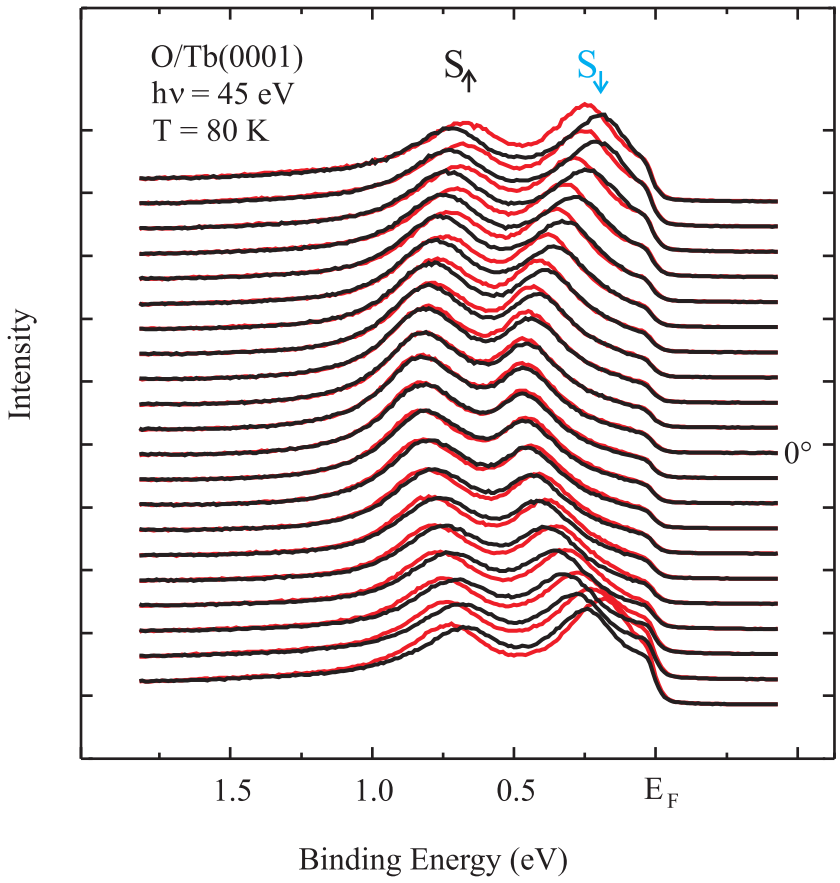

Figure 10.19: (a) Results of a modification of the clean Tb(0001) surface by oxygen adsorption, leading to the formation of a surface-monoxide overlayer. Shown is a set of EDCs, recorded with 45-eV photons. The spectra were recorded in the direction of the $\overline{K} - \overline{\Gamma} - \overline{K}$' azimuth, with angular steps of 0.55° between the spectra.

demonstrates that the Rashba effect is an important surface property of rare-earth metals which has been overlooked in the past. In the present chapter we have presented experimental as well as theoretical evidence for the Rashba effect. With the help of the calculated charge-density contours and the orbital character of the states, we were able to identify the most important contributions to the observed enhancement of the Rashba effect upon surface-oxide layer formation. The previous observation of the Rashba effect on a gold surface, and its absence on the equivalent copper and silver surfaces indicated that the Rashba effect is rather uncommon; with the present work we have discovered a large class of materials that exhibit a sizeable Rashba splitting.

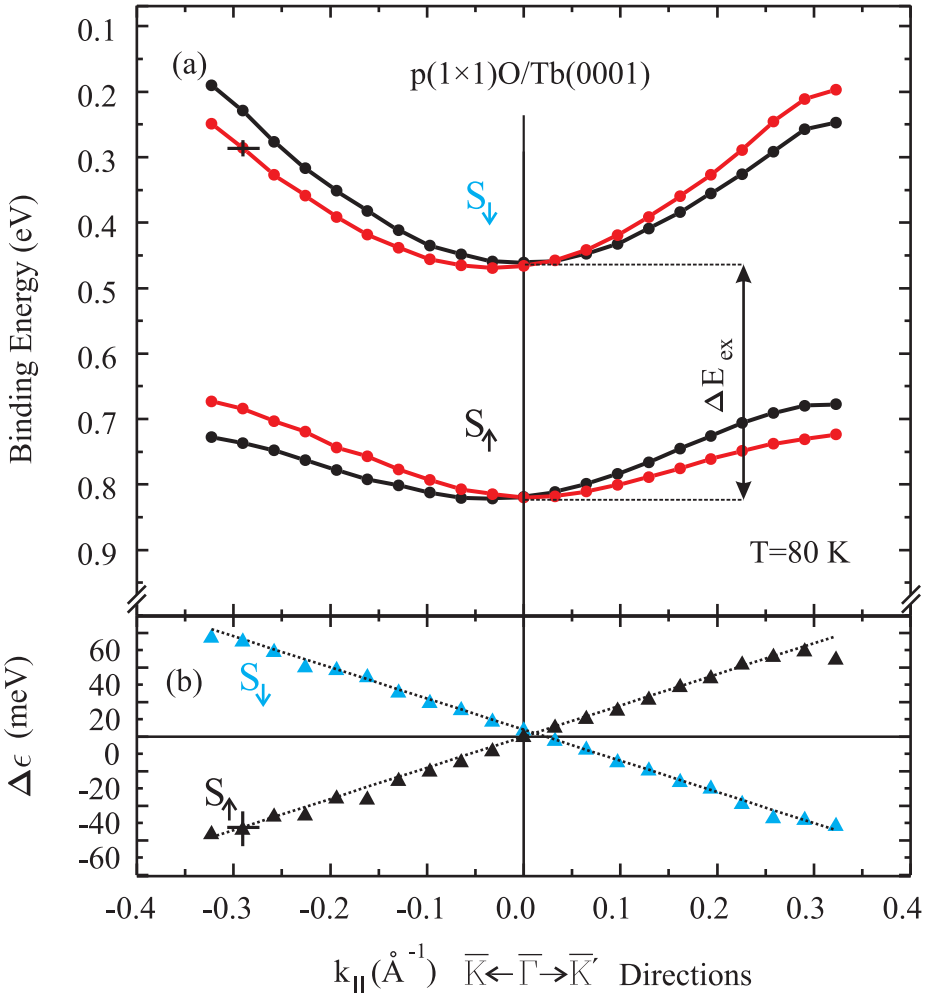

Figure 10.20: (a) Experimentally determined energy dispersion curves for the majority and minority parts of the oxygen-induced surface state on $p(1 \times 1)O/Tb(0001)$. Red and black colors distinguish between opposite magnetization directions; the effect of a magnetization reversal on the dispersion of $p(1 \times 1)O/Tb(0001)$ is clearly observed. (b) Resulting Rashba spin-orbit splitting as the difference in the energy positions measured for the same k value for the two branches.

10.8 Rashba effect and spin structure

In this work we showed experimentally that the spin dependence of the Rashba effect follows our expectations from the Rashba Hamiltonian (see Ex. 9.2). The linear dependence on the spin suggests to utilize this effect on magnetic surfaces as a sensitive probe for the electron spin polarization. The value of the splitting is directly proportional to the projection of the spin on the vector given by the cross-product of the potential gradient and the k vector of the electron. With the gradient being orthogonal to the surface, the maximum Rashba splitting

should occur for orthogonal orientations of spin and k vector. Thus, mapping the Rashba splitting for different electron-propagation ($k-$) directions should give direct experimental access to the spin quantization axis in a 2D system.

One can see that the Rashba shift, for example on clean surfaces of gadolinium an terbium, has the same direction (along the energy and k axis) for a given magnetization direction. In PE experiments, the k value is well defined. Since one can also expect similar electron-charge distributions at all the rare-earth metal surfaces, a reversal of the sign of the potential gradient is unlikely; this means that one can expect the same sign of the Rashba constant. Taking into account the Rashba Hamiltonian, one can conclude that both, the Gd(0001) and Tb(0001) surface, will have the same 5d spin orientation with respect to the 4f spins in the bulk (i.e. parallel or antiparallel). For an absolute calibration, one needs to know the spin polarization in one of the cases (e.g. from an independent measurement). If we assume that Gd(0001) has a ferromagnetic orientation of the surface layer with respect to the bulk, as it is strongly supported by the magnetic dichroism measurements presented in chapter 5, we expect the same situation for the terbium surface.

In general, however, it is necessary to compare the experimental results with the results of theoretical calculations in order to obtain the sign of the Rashba constant. If this information is available, one can unambiguously determine the spin orientation. As an example we consider clean Tb and $p(1\times1)O/Tb(0001)$, where theoretical calculations are required for a conclusive comparison. As shown in Fig. 10.17(a) and Fig. 10.20(a), the Rashba energy shifts of the majority surface states on $p(1\times1)O/Tb(0001)$ reverse sign as compared to the case of Tb(0001). From the Rashba Hamiltonian it is clear that the sign reversal of the Rashba term at a fixed k vector means that either the spin orientation or the Rashba constant has changed sign. Since the sign of the Rashba constant is not available from experiment, we have to resort on the calculations. In view of the very different charge density contours expected for Tb(0001) and for $p(1\times1)O/Tb(0001)$, a sign reversal of the Rashba constant appears rather probable (cf. Gd case Fig. 10.9(a) and Fig. 10.9(b,c)).

It is worthwhile to point out that the Rashba spin-orbit interaction leads to an energy correction of the electronic energy levels; its description as a shift of the bands in k direction is good only in some cases. The sign reversal of the effective mass (upon formation of the surface-monoxide layer) can be rather confusing when using this picture. Comparing the dispersions of the majority states in Fig. 10.17(a) and Fig. 10.20(a), we see that they are shifted in the same k direction (for equal magnetization). Even though at first glance, this seems to be the same Rashba behavior, it is quite different, as shown above. The influence of the effective mass on the sign change of the Rashba shift becomes clear from the sketch in Fig. 10.21. Adding up the linear Rashba term to a concave and convex dispersion curve leads to an effective shift in opposite k directions. Also due to linearity of the Rashba term in k, the resulting energy corrections are different for positive and negative value of the wave vector k. The resulting shifts from the Rashba interaction corrections on the branches of the dispersion curves are indicated by arrows.

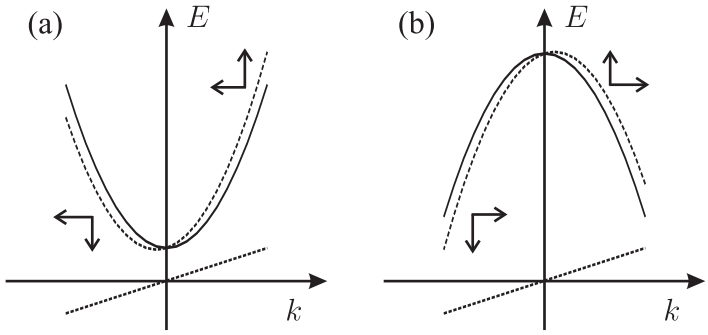

Figure 10.21: Modification of original dispersions (solid lines) by a spin-orbit interaction that is linear in k (dashed straight line) for (a) upward dispersion and (b) downward dispersion. The interaction leads to opposite shifts along the k direction for concave and convex dispersions. The arrows indicate the directions of the shifts of the branches of the resulting dispersion curves (dashed lines) with respect to the original dispersions at different k points.

10.9 Rashba effect versus magnetic dichroism

The Rashba effect and MLD effect have been addressed in detail in the present dissertation. Despite the spin-orbit interaction is the origin of the both effects (resulting in a similar form of the key expressions), their coexistence in photoemission experiments on magnetic surfaces and their resembling appearance at the first glance, the underlying physics is completely different. Thus, it is important to clarify, how to distinguish between them and point out their differences and similarities.

Let us start with their common features. Both effects are caused by spin-orbit interaction and can be observed in the same experimental geometry, shown in Fig. 3.8, using p-polarized light and sample magnetization perpendicular to the excitation plane. Sometimes, as e.g. in case of $O(1 \times 1)/Tb(0001)$, the PE peaks are influenced by both effects at the same time. Necessary conditions for an observation of the MLD effect and the Rashba effect are given by the request for a nonzero value of the following expressions: (i) $(\vec{E} \times \vec{k})\vec{M} \neq 0$ for Rashba effect; (ii) $\vec{E}(\vec{M} \times \vec{k}) \neq 0$ for MLD (chiral experimental geometry). Although these two conditions seem quite similar, the underlying physics is fundamentally different: in the first case, $\vec{E}$ is the electric field vector, whereas in the second case it is the polarization vector of the light.

Moreover, the Rashba Hamiltonian describes the electronic ground state properties of the system, whereas the second condition is imposed on a transition matrix element. The description of the Rashba effect requires only a model of the sample; by contrast, describing an MLD experiment requires a more complex system, including the exciting photon and the photoelectron. In other words, while the Rashba effect modifies the ground-state electronic structure of a solid, the MLD effect can only be observed in the photoexcitation process, as it is shown in chapter 4 of this thesis.

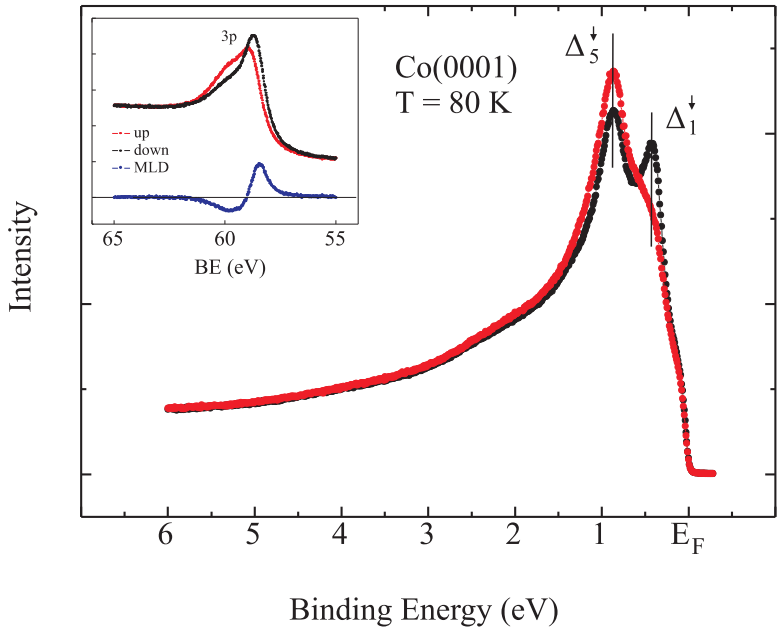

Figure 10.22: Variation of peak intensities due to the MLD effect in the valence-band region observed for a Co(0001) surface upon magnetization reversal. The spectra shown were recorded at normal emission, with the sample cooled to 80 K. The inset presents the MLD effect at the spin-orbit-split 3p-core level. Both spectra were recorded with 130-eV photons.

As we have seen, the Rashba effect results in an k-dependent energy shift of the electronic band dispersion. The MLD effect, on the other-hand, leads to a variation of the intensities of PE peaks. This difference allows one to separate the two effects.

The PE spectra shown in Fig. 10.22 for a magnetic cobalt surface illustrate the MD behavior. The small Z-value (27) of cobalt does not allow to expect a perceptible Rashba effect on its surface, however the MLD effect should be observable in PE experiments. As shown in 10.22, a clear two-peaked structure is resolved, with a substantial intensity variation upon reversal of magnetization. This represents a nice illustration for a pure MLD effect in valence-band PE, which leads to an intensity variation of the PE peaks in strong contrast to the energy shifts of PE peaks due to the Rashba effect (see Fig. 10.19). The spectra of the 3p-core levels of the same film (see inset), show that if the peak structure is not fully resolved, the effect can apparently appear as a shift in energy (i.e. the position of the unresolved peak changes). The consideration of the MLD effect presented in details in chapter 4, shows that such an apparent shift nevertheless originates purely from intensity variations of the spin-orbit split p level.

The high quality of the $p(1\times1)O/Tb(0001)$ data shown in Fig. 10.19, allows one to realize that the PE peaks of the oxygen-induced states are not only subject to the Rashba effect, but exhibit also a sizable MLD effect. The dichroic

behavior of the valence-band states appears as a variation in the intensities of the two Rashba-shifted bands. At normal emission, the spectra match perfectly, giving evidence for a vanishing MLD as well as for a vanishing Rashba effect. For off-normal emission, the minority peak shows an intensity change upon reversal of sample magnetization; for the majority band, this effect is not so pronounced.

It is possible to separate both effects experimentally by the appropriate choice of the PE geometry. Since the Rashba effect does not depend on photon polarization, it is sufficient to change the polarization of the light in order to distinguish from MLD. Changing from p- to s-polarized light, the MLD effect will vanish (see Chapter 4). Orienting $\vec{M}$ parallel to $\vec{k}$ leads to a vanishing Rashba term; in this geometry, however, magnetic dichroism can still be observed with circularly-polarized light (see Chapter 4).